A&A 540, A29 (2012)
DOI: 10.1051/0004-6361/201117845

Astronomy & Astrophysics

A coordinate-independent technique for detecting globally inhomogeneous flat topologies *(Research Note)*

H. Fujii

Institute of Astronomy, School of Science, University of Tokyo, 2-21-1, Osawa, Mitaka, 181-0015 Tokyo, Japan
e-mail: hfujii@ioa.s.u-tokyo.ac.jp

Received 8 August 2011 / Accepted 6 February 2012

ABSTRACT

A flat Universe model that is supported by recent observations can choose among 18 possibilities for its overall topology. To detect or exclude these possibilities is one of the most important tasks in modern cosmology, but it has been very difficult to make for globally inhomogeneous models because of the long time needed for the calculation. In this brief paper we provide an object-based 3D method to overcome the problem, as an extension of Fujii & Yoshii (2011, A&A, 529, A121). Though the test depends on the observer's location in the universe, this method drastically reduces calculation times to constrain inhomogeneous topologies, and will be useful in exhaustively constraining the size of the flat Universe.

Key words. large-scale structure of Universe – cosmology: theory

1. Introduction

The theory of modern cosmology is based on Einstein's general relativity, and recent observations favor a Λ-CDM cosmology with vanishing curvature (e.g., $\Omega_{\rm tot} = 1.0023^{+0.0056}_{-0.0054}$ from WMAP+BAO+SN data, by Jarosik et al. 2011), which successfully describes the observed properties such as the cosmic structure formation, the cosmic microwave background (CMB) anisotropies, and the accelerating expansion. However, General Relativity does not distinguish between two spaces with the same curvature but with different topologies. Though the curvature of our Universe is exactly zero, we still have 18 choices for the overall topology of the Universe (Nowacki 1934), e.g., the multiconnected three-torus $\mathbb{T}^3$ with finite volume. Of these 18 choices, however, 8 topologies are nonorientable and are usually regarded to be physically unacceptable because of arguments of the CPT invariance (Lachièze-Rey & Luminet 1995).

A multiconnected space is a quotient space of the simply connected space with the same curvature ($\mathbb{S}^3$, $\mathbb{E}^3$, or $\mathbb{H}^3$, called covering space), by a holonomy group Γ. It is imagined as a finite or infinite $2K$-polyhedron (the *Dirichlet domain*), whose K pairs of surfaces are connected by the holonomies. Because of these compact dimensions there are many geodesics that connect a given object and the observer, which implies multiple images of single objects, often referred to as "ghosts" (for details, see, e.g., Lachièze-Rey & Luminet 1995). As a result, an observer sees the covering space tessellated by polyhedra ("ghosts" of the Dirichlet domain).

Based on this prediction, many object-based works for exploring cosmic topology were carried out, i.e., one searched for periodic and symmetrical patterns made by ghosts of galaxies, galaxy clusters, or active galactic nuclei (e.g., Sokolov & Shvartsman 1974; Fagundes & Wichoski 1987; Demiański & Łapucha 1987; Lehoucq et al. 1996; Roukema 1996; Uzan et al. 1999; Weatherley et al. 2003; Marecki et al. 2005; Menzies & Mathews 2005; Fujii & Yoshii 2011a,b). Owing to the lack of high-redshift data, object-based methods are normally not suitable for constraining the size of the Universe.

The recent trend is to use CMB data that have the highest redshift available, $z \simeq 1100$. The *circles-in-the-sky* method (Cornish et al. 1998) is a direct method of searching for ghosts of CMB: intersections of the last-scattering surface and our Dirichlet domain. They appear as circles with the same temperature fluctuation pattern in a CMB map since they are physically identical. This method can detect any topologies, but checking all possibilities requires an extremely long-time calculation because of many free parameters: the radius of the matched circles, the celestial positions of centers of the two circles, and the relative phase between the two. The parameter space, however, can be somewhat reduced using the results by Mota et al. (2011).

Exhaustive analyses have not been carried out yet, and various authors searched for matched circles in data limited to antipodal or nearly antipodal ones, using the WMAP satellite's data. Some authors found hints of specific topologies (Poincaré dodecahedral space by Roukema et al. 2008; cubic three-torus by Aurich 2008), while others found no detection and obtained the lower limit of the size of our Universe (Cornish et al. 2004; Key et al. 2007; Bielewicz & Banday 2011). The most recent one is ≥27.9 Gpc by Bielewicz & Banday (2011), which is consistent with the results by Aslanyan & Manohar (2011), who indirectly constrained compact dimensions for three topologies, $\mathbb{T}^3$, $\mathbb{T}^2 \times \mathbb{R}^1$, and $S^1 \times \mathbb{R}^2$, using CMB statistics. These discrepancies could be caused by the methodological problems or by the quality of the CMB map: the signal may be blurred by Doppler, Sachs-Wolfe, or integrated Sachs-Wolfe effects because of the coarse resolution.

Despite the above mentioned results, the possibility that we live in a small universe still remains, because no detection of antipodal (or nearly antipodal) circles puts weaker constraints on the size of inhomogeneous spaces (see Sect. 2.1), e.g., ≥28/3 = 9.3 Gpc for a third-turn space topology and ≥28/4 = 7 Gpc for a quarter-turn space topology. These scales can be explored using

low-redshift (compared to CMB) cosmic objects. In the previous paper we developed an object-based method that can constrain any of the 18 flat topologies with simple algorithms, and is much more sensitive to topological signatures than the preceding ones (Fujii & Yoshii 2011a, hereafter FY11a). Unfortunately, it has a similar problem in checking all possible topologies: calculation times become very long. The aim of this brief paper is to provide a technique, which is valid under some conditions, to overcome the problem. Throughout the paper we consider flat universes, and the calculations were made in comoving coordinates.

2. Method

2.1. Mathematical background and definitions

The mathematical classification of the holonomy groups for flat spaces was completed by Nowacki (1934). Any holonomy γ can be written as $\gamma = \gamma_{\rm T}\gamma_{\rm NT}$, where $\gamma_{\rm T}$ is a parallel translation and $\gamma_{\rm NT}$ is an identity, nth turn rotations (for $n = 2, 3, 4$, or 6), or a reflection. Those spaces whose holonomy groups include only translations ($\gamma_{\rm NT} = id$) are called (globally) homogeneous, all others are called (globally) inhomogeneous. We investigate the latter topologies in this paper.

We write the holonomies in a convenience way using a 4D coordinate system (w, x, y, z) where the simply connected three-Euclidean space $\mathbb{E}^3$ is represented as a hyperplane $w = 1$, so that a usual 3D vector (x, y, z) is represented as a 4D vector $\boldsymbol{x} = (1, x, y, z)$. Every holonomy γ is also written as a 4×4 matrix, e.g., a quarter-turn corkscrew motion is written as

$$\gamma = U \begin{pmatrix} 1 & 0 & 0 & 0 \\ 0 & 0 & -1 & 0 \\ 0 & 1 & 0 & 0 \\ 0 & 0 & 0 & 1 \end{pmatrix} U^{-1} + \begin{pmatrix} 1 & 0 & 0 & 0 \\ L_1 & 0 & 0 & 0 \\ L_2 & 0 & 0 & 0 \\ L_3 & 0 & 0 & 0 \end{pmatrix},$$

where U is a 4×4 matrix representing the choices of the coordinate systems, which reduces to $U = id$ if we choose our z-axis to be parallel to the rotational axis. Hereafter we call this straight line the *fundamental axis* of the holonomy, denoted by $l_{\rm fun}$. The unit vector $\boldsymbol{n}_{\rm fun}$ that is parallel to $l_{\rm fun}$ is called the *fundamental vector*; we identify two antipodal vectors $\boldsymbol{n}_{\rm fun}$ and $-\boldsymbol{n}_{\rm fun}$. For a glide reflection, the fundamental axis $l_{\rm fun}$ is defined to be parallel to the reflectional plane.

In this paper, we continue to consider the same quarter-turn corkscrew motion as an example.

2.2. Summary of the 3D method of FY11a

We review here the FY11a object-based 3D method for detecting cosmic topology (see the paper for details). Our assumption is that the Universe has a spatial section with zero curvature, as suggested by recent observations.

If a pair of comoving objects $\boldsymbol{x}_1$ and $\boldsymbol{x}'_1$ are linked by a holonomy γ, we have by definition

$$\boldsymbol{x}'_1 = \gamma \boldsymbol{x}_1 = \gamma_{\rm T}\gamma_{\rm NT}\boldsymbol{x}_1 = \gamma_{\rm NT}\boldsymbol{x}_1 + \boldsymbol{L}, \quad (1)$$

where $\boldsymbol{L} = (1, L_1, L_2, L_3)$ is the translational vector. Detecting these topological twins requires a parameter search for five parameters: the translational vector $\boldsymbol{L}$ counts for three and the fundamental vector $\boldsymbol{n}_{\rm fun}$ counts for two. To eliminate $\boldsymbol{L}$, we search for two pairs of ghosts (called a *topological quadruplet*) $[(\boldsymbol{x}_1, \boldsymbol{x}_2), (\boldsymbol{x}'_1, \boldsymbol{x}'_2)]$ such that

$$\boldsymbol{x}'_1 = \gamma \boldsymbol{x}_1 = \gamma_{\rm T}\gamma_{\rm NT}\boldsymbol{x}_1 = \gamma_{\rm NT}\boldsymbol{x}_1 + \boldsymbol{L}, \quad (2)$$

$$\boldsymbol{x}'_2 = \gamma \boldsymbol{x}_2 = \gamma_{\rm T}\gamma_{\rm NT}\boldsymbol{x}_2 = \gamma_{\rm NT}\boldsymbol{x}_2 + \boldsymbol{L}. \quad (3)$$

Such a quadruplet always satisfies

$$\boldsymbol{x}'_2 - \boldsymbol{x}'_1 = \gamma_{\rm NT}(\boldsymbol{x}_2 - \boldsymbol{x}_1), \quad (4)$$

independent of $\boldsymbol{L}$. If our z-axis is parallel to the fundamental axis $l_{\rm fun}$ (hence $U = id$), the following relations hold:

$$x'_2 - x'_1 = -(y_2 - y_1), \quad (5)$$

$$y'_2 - y'_1 = x_2 - x_1, \quad (6)$$

$$z'_2 - z'_1 = z_2 - z_1, \quad (7)$$

since γ is a quarter-turn corkscrew motion here.

The FY11a scheme is to search for quadruplets $[(\boldsymbol{x}_i, \boldsymbol{x}_j), (\boldsymbol{x}_k, \boldsymbol{x}_l)]$ that simultaneously satisfy the following three conditions:

1. Separation condition: $|\boldsymbol{x}_i - \boldsymbol{x}_j| = |\boldsymbol{x}_k - \boldsymbol{x}_l|$.
   This condition is common to all holonomies, because holonomies are isometries that preserve distance. Preceding works such as Roukema (1996) and Uzan et al. (1999) also used this mathematical property of holonomies.

2. Vectorial condition: Eqs. (5)–(7).
   This is for a quarter-turn corkscrew motion; for other types of holonomies, see FY11a. A similar condition for a translation was used in Marecki et al. (2005).

3. Lifetime condition: $|t_i - t_k|, |t_j - t_l| < t_{\rm life}$.
   The variables $t_i, t_j, \ldots$ are cosmic times of objects $\boldsymbol{x}_i, \boldsymbol{x}_j, \cdots$, respectively, and $t_{\rm life}$ is the typical lifetime of objects. This condition is important when considering short-lived objects, e.g., active galactic nuclei.

Because of these multifilters, only few ghosts qualify for this test. However, Eqs. (5)–(7) holds only for the specific coordinate system, so we still have to perform the parameter search for two parameters, the fundamental vector $\boldsymbol{n}_{\rm fun}$. To our dismay, this requires more than 10^6 trials, which takes a very long time, since the typical value of the peculiar velocity is 500 km s^{-1}, the quasar lifetime is 10^8 yr, and their distance ~Gpc implies an angular positional uncertainty of $\sim 10^{-3}$. These strong and weak points of the FY11a method is seen in Fig. 1. The integer s is assigned to each object, which is the number of quadruplets including the object as a member, which satisfies all conditions 1–3 (see FY11a for details); topologically lensed objects tend to have high s values. When using the z-axis parallel to $\boldsymbol{n}_{\rm fun}$, some bumps in the histograms are seen that are produced by topological ghosts, while these bumps are not seen when the z-axis deviates from $\boldsymbol{n}_{\rm fun}$. The property of the simulated catalog used here is described in Sect. 3.1.

2.3. Fundamental-vector-searching method

One may aim to have a coordinate-independent filter to extract topological quadruplets, but we found this to be impossible. Consider a quadruplet $[(\boldsymbol{x}_i, \boldsymbol{x}_j), (\boldsymbol{x}_k, \boldsymbol{x}_l)]$ that already satisfies the separation condition and the lifetime condition. It then also satisfies the vectorial condition Eqs. (5)–(7) if we choose the z-axis parallel to a vector $\boldsymbol{n}_{\rm pec}$, seen along which the two vectors $\boldsymbol{a} = \boldsymbol{x}_j - \boldsymbol{x}_i$ and $\boldsymbol{b} = \boldsymbol{x}_l - \boldsymbol{x}_k$ make a right angle (Fig. 2). The unit vector $\boldsymbol{n}_{\rm pec}$ is called *peculiar vector* of the quadruplet, for a quarter-turn corkscrew motion.

We consider the quarter-turn corkscrew motion as an example throughout the paper, but treatments of the other types of holonomies are the same except for the step 3. The peculiar axis

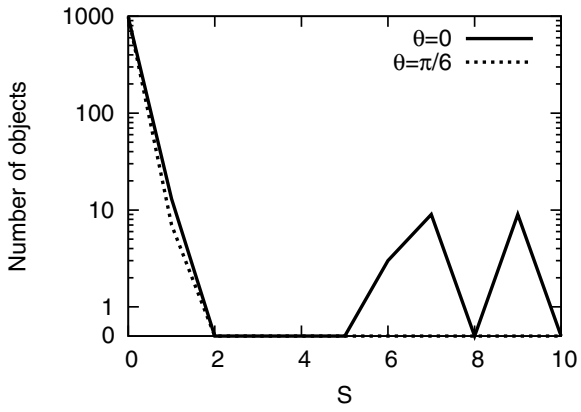

Fig. 1. Solid line: the result using the z-axis parallel to $\boldsymbol{n}_{\rm fun}$. Broken line: the result using the z-axis that is at an angle of $\pi/6$ with $\boldsymbol{n}_{\rm fun}$. The catalog used here consists of 1008 objects including 10 pairs of ghosts, and the observer stands at a distance of 1.75 Gpc from $l_{\rm fun}$ (see Sect. 3.2). Vertical scale is linear from 0 to 1 and logarithmic from 1 to 1000.

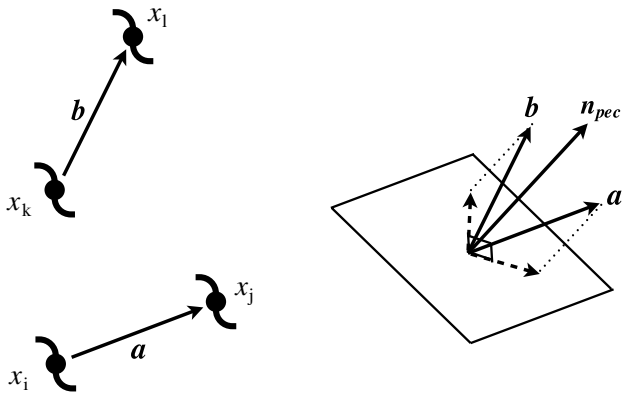

Fig. 2. Even a nontopological quadruplet seems to be linked by a quarter-turn corkscrew motion when we choose the z-axis parallel to its peculiar axis $\boldsymbol{n}_{\rm pec}$.

of the quadruplet $[(\boldsymbol{x}_i, \boldsymbol{x}_j), (\boldsymbol{x}_k, \boldsymbol{x}_l)]$ for each type of holonomies can be defined as follows.

1. Nth turn corkscrew motions. In this case the fundamental axis is defined to be parallel to the rotational axis. The apparent angle between $\boldsymbol{a}$ and $\boldsymbol{b}$, therefore, should be $2\pi/n$ when seen from its peculiar vector $\boldsymbol{n}_{\rm pec}$. This vector is obtained by rotating the unit vector parallel to $\boldsymbol{a} + \boldsymbol{b}$ around the axis parallel to $\boldsymbol{a} - \boldsymbol{b}$ by the angle of

$$\alpha = \pm \arcsin\left(\frac{\tan\phi}{\tan\frac{\pi}{n}}\right), \tag{8}$$

where ϕ is half the intrinsic angle between $\boldsymbol{a}$ and $\boldsymbol{b}$. The quadruplet with $\phi > \pi/n$ has no peculiar axes, which never occurs when $n = 2$ (half-turn corkscrew motion).

2. Glide reflections. In this case the fundamental axis is defined to be perpendicular to the reflectional plane, hence the peculiar vector is the unit vector parallel to $\boldsymbol{a} - \boldsymbol{b}$.

Therefore, it is impossible to judge whether a given quadruplet is topological, however, if there really exists a fundamental axis (and vector) in the Universe, there should be more quadruplets whose peculiar vectors are parallel to it than stochastically expected. To detect such an excess alignment is the essential idea of the coordinate-independent technique described here. The detailed procedure, which hereafter we call the "fundamental-vector-searching (FVS)" method, works as follows.

1. The celestial sphere is divided into $12N_{\rm side}^2$ equal area pixels. Because we identify two antipodal vectors, the number of pixels used is $6N_{\rm side}^2$.
2. The quadruplets that satisfy both the separation condition and the lifetime condition are selected.
3. For each selected quadruplet, its peculiar vector $\boldsymbol{n}_{\rm pec}$ and the pixel containing $\boldsymbol{n}_{\rm pec}$ within it is calculated.
4. For each object $\boldsymbol{x}_i$, we flag pixels that contain more than $s_{\rm min}$ peculiar axes of the quadruplets that include $\boldsymbol{x}_i$.
5. Each pixel is assigned an integer with the number of times that it was flagged in the previous step.

These steps practically correspond to counting the number of objects with $s_i > s_{\rm min}$ for all possible z-axes. Note that the choices of the parameters $N_{\rm side}$ and $s_{\rm min}$ are not independent; a small $N_{\rm side}$ corresponds to large pixels and large stochastic noises, so $s_{\rm min}$ should be chosen to be large enough. We used the HEALPix scheme (Górski et al. 2005) for the pixelization of the celestial sphere.

3. Simulations and discussions

3.1. Details of simulated catalogs

To demonstrate how the FVS method works, we applied the method to catalogs of toy quasars. The details of the simulations are as follows.

- The standard Λ-CDM cosmology ($\Omega_{\rm m} = 0.27, \Omega_\Lambda = 0.73, H_0 = 71$ km s^{-1} Mpc^{-1}) was used so that the local geometry is Euclidean.
- A quarter-turn space topology was assumed such that the detectable holonomies are only two quarter-turn corkscrew motions. The translational distance of these detectable holonomies is $L = 7$ Gpc, which is consistent with the negative results on homogeneous topologies using the WMAP data (see Sect. 1).
- We used a full sky and shell-like catalog: 3.5 Gpc $(L/2) < r <$ 5.25 Gpc $(3L/4)$ in comoving radius, or $1.1 \lesssim z \lesssim 2.0$ in redshift.
- The objects are distributed uniformly in the comoving space.
- The quasar luminosity evolution was simplified such that they emit radiation with a constant luminosity during the fixed duration $t_{\rm life} = 10^8$ yr.
- The peculiar motion was simplified to move with a constant speed $v = 500$ km s^{-1} and with randomly chosen directions.
- Other natures of quasars and technical uncertainties were all ignored.

We acknowledge that these simple assumptions are not suitable for practical applications; the aim here is just to show the essence of the test.

3.2. Main results: detection of the fundamental axis

First we applied the FY11a method to a toy quasar catalog seen from an observer standing at a comoving distance of $r_{\rm obs} = 1.75$ Gpc $(L/4)$ from $l_{\rm fun}$. The catalog contains 1008 objects, including 10 pairs of ghosts. Two choices of coordinate systems were used, $\theta = 0$ and $\pi/6$, where θ is the angle between the chosen z-axis and $\boldsymbol{n}_{\rm fun}$. These results are given in Fig. 1 and were

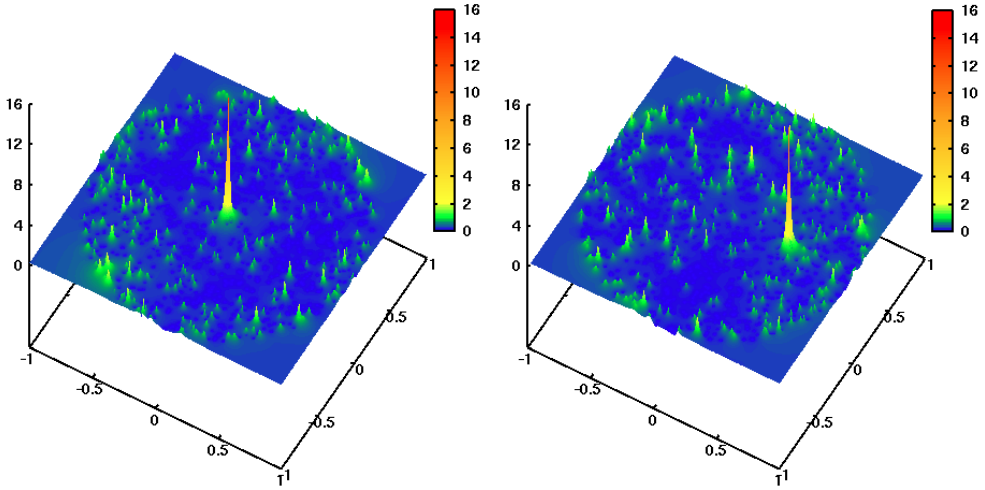

Fig. 3. Fundamental vector $\boldsymbol{n}_{\rm fun}$ appears as a sharp peak in both cases; *left*: $\theta = 0$, *right*: $\theta = \pi/6$. The observer stands at a distance of 1.75 Gpc from the fundamental axis $l_{\rm fun}$.

already discussed; the topological signal appears only for the former case ($\theta = 0$), and we generally have to change our z-axis as free parameters to detect globally inhomogeneous topologies (see also Sect. 5.2.1 of FY11a). This takes an extremely long time, which motivated us to commence this work.

Next we applied the FVS method to the same catalog using $N_{\rm side} = 500$ and $s_{\rm min} = 2$. If there is a topological quadruplet, its peculiar vector $\boldsymbol{n}_{\rm pec}$ ideally coincides with the fundamental vector $\boldsymbol{n}_{\rm fun}$, but not in practice because of the peculiar motions. The resolution parameter $N_{\rm side}$ is determined so that it covers this positional deviations. The cutoff parameter $s_{\rm min} = 2$ is a reasonable choice because the quadruplets with $s_i > 2$ seem to rarely occur by chance, as can be seen in Fig. 1 (broken line).

The results are shown as 2D color histograms (Fig. 3), where half the celestial sphere is orthogonally projected onto the xy-plane. As expected, a pixel containing the fundamental axis has more counts than the other pixels, whose counts are purely stochastic, independently of the coordinate systems.

This single calculation takes about a few minutes with a present-day ordinary personal computer, and is equivalent to performing about $\sim 10^6$ trials of the FY11a method, which takes about one year. This is the notable advantage of the FVS method over the other methods, e.g., the CMB-based circles-in-the-sky method that cannot constrain all possible topologies in a reasonable time.

3.3. Limits of the method: observer's location

The results of the previous section are based on somewhat idealized assumptions. In practice, there are various effects to be considered correctly: physical properties of astronomical objects and observational uncertainties. These effects will be treated in forthcoming papers and not here, but there is another important factor that affects this test; the limit of the FVS method depends on the observer's location in the universe.

For there to be a sharp peak, the following two conditions must be satisfied:

1. all peculiar vectors $\boldsymbol{n}_{\rm pec}$ of topological quadruplets are lying in one (or a few) pixel;
2. the stochastic noise contained in one pixel is much less than the topological signal.

The first condition requires a sufficiently large pixel size, while the second condition requires a sufficiently small pixel size. Consequently, one needs to find a good balance between them, however, this becomes impossible for an observer "near" the fundamental axis $l_{\rm fun}$.

To see this effect, let us consider a topological quadruplet $[(\boldsymbol{x}_i, \boldsymbol{x}_j), (\boldsymbol{x}'_i, \boldsymbol{x}'_j)]$, which satisfies

$$a_x = -b_y + \varepsilon_x, \tag{9}$$
$$a_y = b_x + \varepsilon_y, \tag{10}$$
$$a_z = b_z + \varepsilon_z, \tag{11}$$

where $\boldsymbol{a} = \boldsymbol{x}_j - \boldsymbol{x}_i$, $\boldsymbol{b} = \boldsymbol{x}'_j - \boldsymbol{x}'_i$, and $\boldsymbol{\varepsilon}$ represents the positional perturbations due to peculiar motions. The coordinate system is chosen so that the z-axis corresponds to $l_{\rm fun}$. To calculate the peculiar vector of this quadruplet, we need two vectors $\boldsymbol{a}+\boldsymbol{b}$ and $\boldsymbol{a}-\boldsymbol{b}$ (Sect. 2.3):

$$\boldsymbol{a}+\boldsymbol{b} = (a_x + a_y - \varepsilon_y, a_y - a_x + \varepsilon_x, 2a_z + \varepsilon_z), \tag{12}$$

$$\boldsymbol{a}-\boldsymbol{b} = (a_x - a_y + \varepsilon_y, a_y + a_x - \varepsilon_x, -\varepsilon_z), \tag{13}$$

whose directions are highly perturbed from the unperturbed ones if $a_x + a_y, a_x - a_y$, or a_z are comparable to $\boldsymbol{\varepsilon}$. Indeed, a_z systematically takes low values if the surfaces of the Dirichlet domain are nearly perpendicular to $l_{\rm fun}$ when using short-lived objects such as quasars and starburst galaxies, which are luminous and suitable for high-redshift observations, since their ghosts appear close to (on the order of $\sim ct_{\rm life}$) the surfaces. The angle between the Dirichlet domain surface and $l_{\rm fun}$ is given by $\arctan(L/\sqrt{2}r_{\rm obs})$, so this situation occurs when $r_{\rm obs}/L \ll 1$. For such an observer it is hard to find a good compromise between the two conditions.

Therefore, if the Milky Way happens to be situated near $l_{\rm fun}$ compared to L, the FVS method can no longer detect topological signatures and a troublesome parameter search of FY11a method (or other possible methodologies) is needed. For example, we generated a toy quasar catalog seen from the observer standing along $l_{\rm fun}$. The catalog contains 996 objects including 11 pairs of ghosts. In Fig. 4, it can be seen that the FVS method

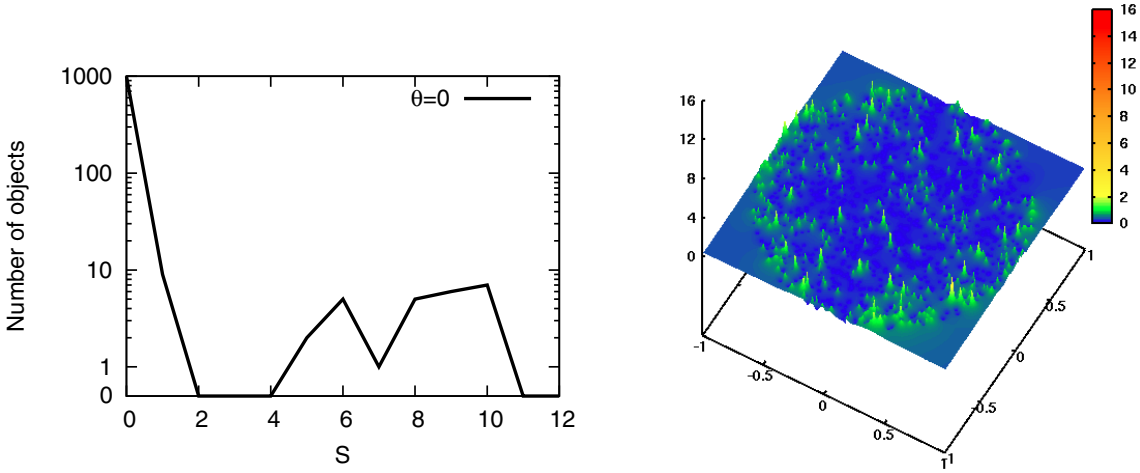

Fig. 4. If the observer stands along $l_{\rm fun}$, the FVS method does not work well (*right*) and a tremendous parameter search of the FY11a method is necessary (*left*). A sharp peak at $(0, 0)$ is leveled because of the high dispersion of $\boldsymbol{n}_{\rm pec}$ of topological quadruplets.

does not detect the fundamental vector, while the FY11a method successfully detects the topological signature, although in practice a prolonged calculation to search for $\boldsymbol{n}_{\rm fun}$ is needed.

We have seen what happens when $r_{\rm obs}/L \ll 1$, however, there is another effect of the observer's location, which is that the distance d to the Dirichlet domain surfaces is a monotonically increasing function of $r_{\rm obs}$ (see also Sect. 5.2.2 of FY11a). For a half-turn corkscrew motion it is given by

$$d = \frac{1}{2}\sqrt{2r_{\rm obs}^2 + L^2}. \tag{14}$$

When $r_{\rm obs}$ is larger than a certain value the observed region is entirely contained in the Dirichlet domain, which implies no ghost images. In contrast to the former effect, in this case any other direct method, which is to search for topological ghosts, is also invalid.

3.4. Summary and prospects

We introduced an object-based method (FVS method) that is able to enhance the lower limit on the size of the Universe for inhomogeneous flat topologies. If the Universe has a fundamental axis $l_{\rm fun}$ (or vector $\boldsymbol{n}_{\rm fun}$) and sufficiently small dimension, topological quadruplets tend to align with it, as can be seen in Fig. 3 (sharp spikes). This is a parameter-free extension of FY11a method, which treated $\boldsymbol{n}_{\rm fun}$ as free parameters.

However, for a practical application we need more realistic simulations. Therefore our next work will focus on these problems: detailed treatments on physical properties of astronomical objects and technical uncertainties of observations. When this is accomplished, we will be able to apply the FVS method to the observed catalogs of our real Universe. Recent and future large-scale survey projects, such as 2dFGRS (Croom et al. 2004), SDSS (Schneider et al. 2010), the Large Synoptic Survey Telescope (LSST), and the Joint Astrophysics Nascent Universe Satellite (JANUS) will provide sufficient data for this test. The formidable progress in techniques for measuring photometric redshifts suggests that the spectroscopic surveys are not necessarily needed, which makes the application more realistic.

Acknowledgements. I gratefully acknowledge Y. Yoshii for his various supports, useful discussions and constructive suggestions. I also thank M. Doi, T. Minezaki, T. Tsujimoto, T. Yamagata, T. Kakehata, K. Hattori, and T. Shimizu for useful discussions and suggestions. Finally, I thank the referee for careful reading of the paper and for constructive suggestions. Some of the results in this paper were derived using the HEALPix package.

References

Aslanyan, G., & Manohar, A. V. 2011 [arXiv:1104.0015]
Aurich, R. 2008, Class. Quant. Grav., 25, 225017
Aurich, R., & Lustig, S. 2011, Class. Quant. Grav., 28, 085017
Bielewicz, P., & Banday, A. J. 2011, MNRAS, 412, 2104
Cornish, N. J., Spergel, D. N., & Starkman, G. D. 1998, Class. Quant. Grav., 15, 2657
Cornish, N. J., Spergel, D. N., Starkman, G. D., & Komatsu, E. 2004, Phys. Rev. Lett., 92, 201302
Croom, S. M., Smith, R. J., Boyle, B. J., et al. 2004, MNRAS, 349, 1397
Demianski, M., & Lapucha, M. 1987, MNRAS, 224, 527
Fagundes, H. V., & Wichoski, U. F. 1987, ApJ, 322, L5
Fan, X., Strauss, M. A., Schneider, D. P., et al. 2001, AJ, 121, 54
Fujii, H., & Yoshii, Y. 2011a, A&A, 529, A121
Fujii, H., & Yoshii, Y. 2011b, A&A, 531, A171
Górski, K. M., Hivon, E., Banday, A. J., et al. 2005, ApJ, 622, 759
Ivezic, Z., Tyson, J. A., Acosta, E., et al. 2008, unpublished [arXiv:0805.2366]
Key, J. S., Cornish, N. J., Spergel, D. N., & Starkman, G. D. 2007, Phys. Rev. D, 75, 084034
Lachieze-Rey, M., & Luminet, J. 1995, Phys. Rep., 254, 135
Lehoucq, R., Lachieze-Rey, M., & Luminet, J. P. 1996, A&A, 313, 339
Lehoucq, R., Uzan, J., & Luminet, J. 2000, A&A, 363, 1
Lew, B., & Roukema, B. 2008, A&A, 482, 747
Linde, A. 2004, J. Cosmol. Astropart. Phys., 10, 4
Marecki, A., Roukema, B. F., & Bajtlik, S. 2005, A&A, 435, 427
Menzies, D., & Mathews, G. J. 2005, J. Cosmol. Astropart. Phys., 10, 8
Mota, B., Rebouças, M. J., & Tavakol, R. 2010, Phys. Rev. D, 81, 103516
Nowacki, W. 1934, Comment. Math. Helvet., 7, 81
Roming, P. 2008, in COSPAR, Plenary Meeting, 37th COSPAR Scientific Assembly, 37, 2645
Roukema, B. F. 1996, MNRAS, 283, 1147
Roukema, B. F., Lew, B., Cechowska, M., Marecki, A., & Bajtlik, S. 2004, A&A, 423, 821
Roukema, B. F., Buliński, Z., & Gaudin, N. E. 2008a, A&A, 492, 657
Roukema, B. F., Buliński, Z., Szaniewska, A., & Gaudin, N. E. 2008b, A&A, 486, 55
Schneider, D. P., Richards, G. T., Hall, P. B., et al. 2010, AJ, 139, 2360
Uzan, J., Lehoucq, R., & Luminet, J. 1999, A&A, 351, 766
Weatherley, S. J., Warren, S. J., Croom, S. M., et al. 2003, MNRAS, 342, L9